First microscopic coupled-channels calculation of cross sections for inelastic α scattering off ^{16}O

Yoshiko Kanada-En'yo

Department of Physics, Kyoto University, Kyoto 606-8502, Japan

Kazuyuki Ogata

Research Center for Nuclear Physics (RCNP), Osaka University, Ibaraki 567-0047, Japan;
Department of Physics, Osaka City University, Osaka 558-8585, Japan;
and Nambu Yoichiro Institute of Theoretical and Experimental Physics (NITEP), Osaka City University, Osaka 558-8585, Japan

The α inelastic scattering on ^{16}O is investigated with the coupled-channels calculation using the α-nucleus coupled-channels potentials, which are microscopically derived by folding the the Melbourne g-matrix NN interaction with the ^{16}O and α densities. The matter and transition densities of ^{16}O are calculated by a microscopic structure model of the variation after the spin-parity projections combined with the generator coordinate method of ^{12}C + α in the framework of the antisymmetrized molecular dynamics. The calculation reproduces the observed elastic and inelastic cross sections at incident energies of $E_\alpha = 104$, 130, 146, and 386 MeV. The coupled-channels effect on the cross sections is also discussed.

I. INTRODUCTION

The α scattering has been used for the study of isoscalar (IS) monopole and dipole excitations in nuclei. The inelastic cross sections have been analyzed by reaction model calculations to determine the strength functions in a wide range of excitation energy covering the giant resonances [1]. The α scattering is also a good tool to probe cluster states because these have generally strong IS monopole and dipole transition strengths and can be populated by the α-scattering reaction [2–4]. Indeed, the (α, α') reaction experiments have been intensively performed to investigate cluster structures of excited states in light nuclei such as ^{12}C and ^{16}O recently.

For the study of cluster structures in ^{12}C, the ^{12}C(α, α') reaction has been investigated with reaction models [5–12], but many of the reaction calculations encountered the overshooting problem of the 0_2^+ cross sections. Also for sd-shell nuclei such as ^{16}O, α-scattering experiments have reported the similar overshooting problem of the 0^+ cross sections in the reaction model analysis [12]. Recently, Minomo and one of the authors (K.O.) have carried out microscopic coupled-channels calculation and succeeded in reproducing the 0_2^+ cross sections of the ^{12}C(α, α') reaction with no adjustable parameter [13]. In the study, α-nucleus coupled-channel (CC) potentials are constructed by folding the Melbourne g-matrix effective NN interaction [14] by a phenomenological matter density of α and the matter and transition densities of ^{12}C obtained with the resonating group method [15]. In our previous paper [16], we have applied the g-matrix folding model to the same reaction and reproduced the cross sections of the $0_{2,3}^+$, 1_1^-, $2_{1,2}^+$, and 3_1^- states of ^{12}C with the transition density obtained by the antisymmetrized molecular dynamics (AMD) [17–21], which is a microscopic structure model beyond the cluster models. These works indicate that, if reliable transition

densities are available from structure model calculations, then the approach of the g-matrix folding model can be a useful tool to investigate cluster states by the (α, α') reaction.

In the structure studies of ^{16}O, a variety of cluster structures such as the 4α-tetrahedral, ^{12}C + α, and a 4α-cluster gas state have been suggested by the cluster models [3,22–38]. Recently, the experimental studies of ^{16}O have been performed by the ^{16}O(α, α') reaction [12,39]. In Ref. [39], the 0_4^+ state at 13.6 MeV has been discussed in relation with the 4α-gas state with the reaction model analysis using phenomenological CC potentials. In the study, the α-scattering cross sections are naively assumed to scale the IS monopole strengths.

However, no microscopic CC calculation of the ^{16}O(α, α') reaction was performed so far, mainly because of the theoretical difficulty of microscopic structure models in the description of ^{16}O. For instance, a well-known problem is that microscopic cluster models largely overshoot the excitation energy of the $K^\pi = 0_2^+$ band. Recently, one of the authors (Y.K.-E.) investigated the cluster structures of ^{16}O [40–42] with the AMD. She has performed the variation after spin-parity projections (VAP) combined with the generator coordinate method (GCM) of the ^{12}C + α cluster in the AMD framework, which we called the VAP + GCM. The VAP + GCM calculation qualitatively described the energy spectra of ^{16}O and obtained the 0_2^+, 2_1^+, 4_1^+, 1_2^-, and 3_2^- states in the ^{12}C + α bands and the 3_1^- and 4_2^+ states in the 4α-tetrahedral ground band. Moreover, it predicts the 4α-gas state as the 0_5^+ state near the 4α threshold energy.

In this paper, we apply the g-matrix folding model to the ^{16}O(α, α') reaction using the matter and transition densities calculated with the VAP + GCM in a similar way to in our previous work on the ^{12}C(α, α') reaction [16]. The present work is the first microscopic CC calculation of the ^{16}O(α, α')

reaction that is based on the microscopic α-nucleus CC potentials derived with the g-matrix folding model. The calculated cross sections are compared with the observed data at incident energies of $E_\alpha = 104$, 130, 146, and 386 (400) MeV [12,39,43–45]. The IS monopole and dipole transitions to the $0^+_{2,3,4,5}$ and 1^-_1 states are focused. We try to answer the following questions. Can the microscopic reaction calculation describe the α-scattering cross sections? Does the overshooting problem of the monopole strength exist? Is the scaling law of the α-scattering cross sections and the IS monopole transition strength satisfied?

The paper is organized as follows. Section II describes the structure calculation of ^{16}O with the VAP + GCM, and Sec. III discusses the ^{16}O(α, α') scattering investigated with the microscopic CC calculation. Finally, a summary is given in Sec. IV.

II. STRUCTURE CALCULATION OF ^{16}O WITH VAP + GCM

A. Wave functions of ^{16}O

The wave functions of ^{16}O are those obtained by the VAP [19] combined with the ^{12}C $+ \alpha$ GCM in the AMD framework, which we called the VAP + GCM [41]. As shown in Ref. [42], the VAP + GCM calculation reasonably reproduces the energy spectra and transition strengths of ^{16}O and obtains various cluster structures such as the 4α and ^{12}C $+ \alpha$ cluster structures. For the details of the formulation of the structure calculation and the resulting structures and band assignments in ^{16}O, the reader is referred to Refs. [40–42]. Using the VAP + GCM wave functions, the transition strengths, matter and transition densities, and form factors are calculated. The definitions of these quantities are given in Refs. [16,42].

B. Excitation energies and radii

The excitation energies and radii of ^{16}O from the VAP + GCM calculation and the experimental data are listed in Table I. We assign the fourth 0^+ (0^+_{IV}), the third 0^+ (0^+_{III}), the third 2^+ (2^+_{III}), and the second 2^+ (2^+_{II}) states in the theoretical spectra to the experimental levels of the 0^+_3 (12.05 MeV), 0^+_4 (13.6 MeV), 2^+_2 (9.85 MeV), and 2^+_3 (11.52 MeV) states, respectively, because the VAP + GCM calculation gives incorrect ordering of the $K^\pi = 0^+_3$ and 0^+_4 bands; for a detailed discussion, see Ref. [40]. The nuclear sizes of the 3^-_1 and 1^-_1 states are comparable to the ground state and relatively smaller than those of other excited states because the 3^-_1 is the 4α-tetrahedral state in the ground band and the 1^-_1 is the vibration mode on the tetrahedral ground band. The 4^+_2 state is also regarded as the 4α-tetrahedral band but its size is slightly larger than those of the other two in the ground band because of the mixing with the 4^+_1 state in the ^{12}C $+ \alpha$ cluster band. Other states are developed cluster states and have relatively larger radii than those of the ground-band states. The density distribution of the $0^+_{1,2,3,4,5}$, $1^-_{1,2}$, $2^+_{1,2,3}$, $3^-_{1,2}$, and $4^+_{1,2}$ states obtained by the VAP + GCM is shown in Fig. 1. The $0^+_{2,3,4,5}$, 1^-_2, $2^+_{1,2,3}$, 3^-_2, and 4^+_1 states tend to have the

TABLE I. Excitation energies E_x (MeV) and rms matter radii R (fm) of ^{16}O calculated with the VAP+GCM. The experimental values of the excitation energies from Ref. [46] are also shown. The experimental data $R = 2.55$ fm of the rms radius of the ground state is deduced from the experimental charge radius measured by the electron scattering [47]. We assign the fourth 0^+, third 0^+, third 2^+, and the second 2^+ states obtained by the VAP+GCM to the experimental 0^+_3, 0^+_4, 2^+_2, and 2^+_3 states, which we label as $0^+_{3,IV}$, $0^+_{4,III}$, $2^+_{2,III}$, and $2^+_{3,II}$, respectively.

	Expt.	VAP+GCM	
	E_x (MeV)	E_x (MeV)	R (fm)
0^+_1	0	0.0	2.73
0^+_2	6.0494	9.7	3.29
$0^+_{3,IV}$	12.049	15.3	3.53
$0^+_{4,III}$	13.6	13.6	3.64
0^+_5	14.01	18.3	3.53
2^+_1	6.917	10.8	3.27
$2^+_{2,III}$	9.846	14.7	3.37
$2^+_{3,II}$	11.52	14.0	3.51
2^+_4	13.04	16.1	3.55
2^+_5	14.926	16.9	3.26
2^+_6	15.26	18.9	3.56
2^+_7	16.44	20.3	3.86
2^+_8	16.93	20.6	3.38
4^+_1	10.356	13.7	3.34
4^+_2	11.097	14.5	3.18
4^+_3	13.869	16.6	3.63
1^-_1	7.1169	9.4	2.87
1^-_2	9.585	12.1	3.58
3^-_1	6.1299	7.6	2.78
3^-_2	11.600	13.4	3.65

slightly enhanced surface density in the range of $r = 4$–5 fm because of the developed cluster structures.

C. Transition strengths, transition densities, and charge form factors of ^{16}O

In Table II, the transition strengths, $B(E\lambda)$, of ^{16}O calculated with the VAP + GCM are shown compared with the experimental data. For the IS dipole transition strengths of the $1^- \to 0^+$ transitions, the values of $B(\text{IS}1)/4$ are shown. The energy levels and the major $E2$ transitions are shown in Fig. 2. In the figure, the energy levels are connected by (green) dashed and (red) solid lines for the case of remarkable $E2$ transitions of $50 < B(E2) < 100$ e^2 fm^4 and $B(E2) > 100$ e^2 fm^4, respectively. Rather strong $E2$ transitions are found for developed cluster states. Some of those remarkable $\lambda = 2$ transitions give significant CC effects to the α-scattering cross sections as discussed later. The $K^\pi = 0^+_2$ band of the ^{12}C $+ \alpha$ cluster is composed of the 0^+_2, 2^+_1, and 4^+_1 states, and its parity partner $K^\pi = 0^-$ band is constructed
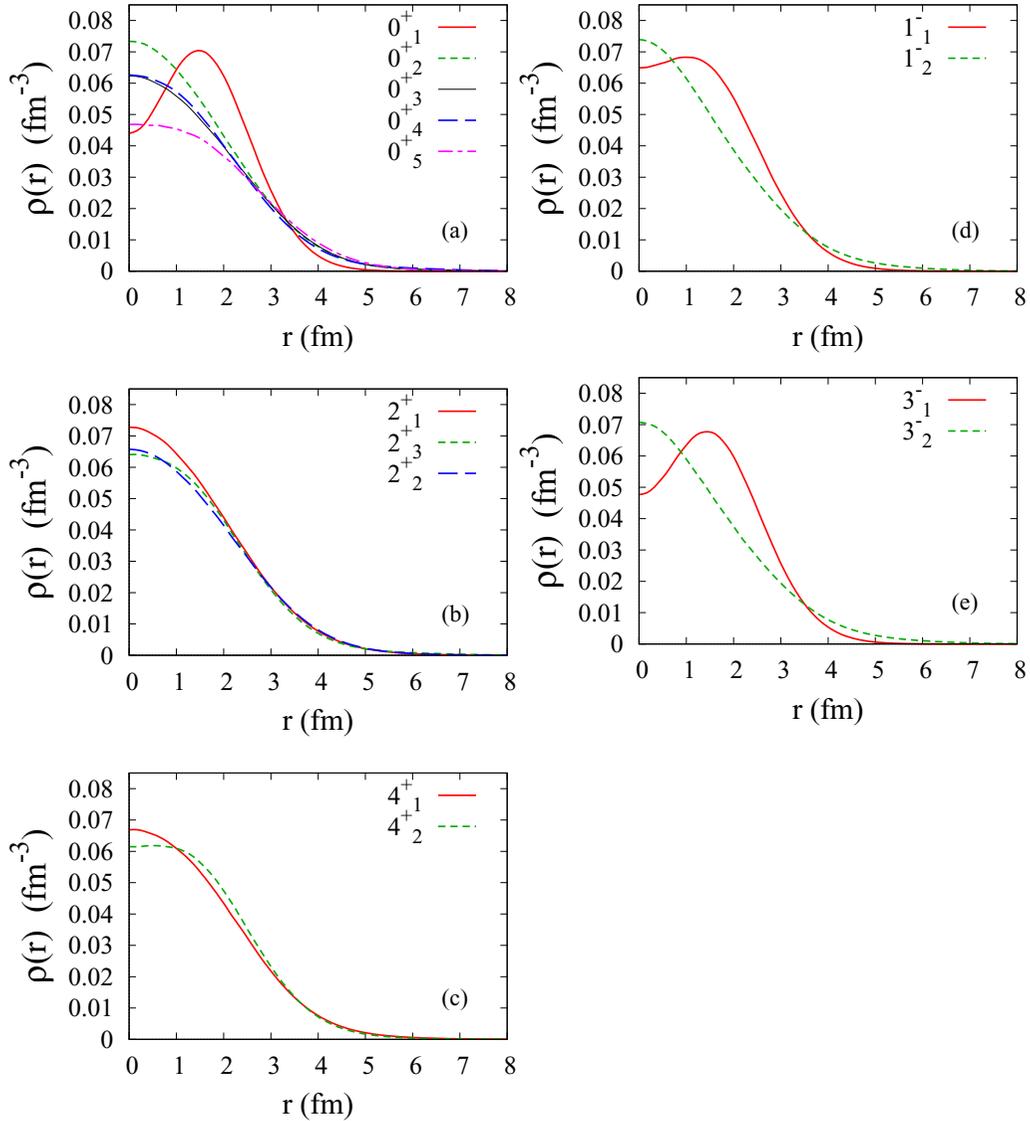
FIG. 1. Proton density $\rho_p(r) = \rho(r)/2$ of the $0^+_{1,2,3,4,5}$, $1^-_{1,2}$, $2^+_{1,2,3}$, $3^-_{1,2}$, and $4^+_{1,2}$ states of ^{16}O calculated with the VAP + GCM.

by the 1^-_2 and 3^-_2 states. The 4α-gas state is obtained as the 0^+_5 state.

To reduce ambiguity from the structure model calculation in application of the theoretical transition density to the reaction calculation, we scale the calculated result as $\rho^{(\mathrm{tr})}(r) \to f_{\mathrm{tr}}\rho^{(\mathrm{tr})}(r)$ to fit the observed $B_{\exp}(E\lambda)$. The scaling factor $f_{\mathrm{tr}} = \sqrt{B_{\exp}(E\lambda)/B_{\mathrm{cal}}(E\lambda)}$ introduced here is defined by the square root of the ratio of the experimental $B(E\lambda)$ value to the theoretical one. The adopted value of f_{tr} for each transition is shown in Table II. For the transitions for which experimental data of $B(E\lambda)$ do not exist, we take $f_{\mathrm{tr}} = 1$ and use the original transition density. For the $1^-_1 \to 0^+_1$ transition, $B(\mathrm{IS}1)$ is unknown, but the charge form factors are available from the (e, e') reaction data. For this transition, we use $f_{\mathrm{tr}} = 1$ in the default CC calculation, and also test a modified value $f_{\mathrm{tr}} = 1.3$ of the $0^+_1 \to 1^-_1$ transition density, which consistently reproduces the charge form factors and α-scattering

cross sections. Figure 3 shows the scaled transition density $f_{\mathrm{tr}}\rho^{(\mathrm{tr})}(r)$ for transitions from the ground state.

We show in Fig. 4 the charge form factors of ^{16}O calculated with the VAP + GCM and the experimental data measured by the electron scattering [48]. The calculated form factors are scaled by multiplying f_{tr}^2 consistently with the scaled transition density. The experimental data are reasonably reproduced by the scaled form factors of the VAP + GCM. In the $E2$ form factors of the 2^+ states [Fig. 4(d)], a clear difference can be seen in the $0^+_1 \to 2^+_2$ from the other $E2$ transitions of $0^+_1 \to 2^+_{1,3}$ because the corresponding transition density of $0^+_1 \to 2^+_2$ shows the different behavior that it is the compact spatial distribution with no nodal structure [see Fig. 3(b)]. In the $E0$ form factors of 0^+ states, the $0^+_1 \to 0^+_2$ transition has the dip at the smallest momentum transfer (q^2) corresponding to the broadest distribution of the transition density.

TABLE II. The transition strengths $B(E\lambda)$ of ^{16}O calculated with the VAP+GCM and the experimental data from Refs. [46,48]. For the IS dipole transition strengths of the $1^- \to 0^+$ transitions, the values of $B(\mathrm{IS1})/4$ are shown. The scaling factor $f_{\mathrm{tr}} = \sqrt{B_{\mathrm{exp}}(E\lambda)/B_{\mathrm{cal}}(E\lambda)}$ determined by the ratio of the experimental value $B_{\mathrm{exp}}(E\lambda)$ to the calculated value $B_{\mathrm{cal}}(E\lambda)$ for each transition is also shown. For the transitions with no experimental data of $B(E\lambda)$, $f_{\mathrm{tr}} = 1$ is used. The units are $e^2\,\mathrm{fm}^{2\lambda}$ for $B(E\lambda)$ ($\lambda \neq 0$), $e^2\,\mathrm{fm}^4$ for $B(E0)$, and fm^6 for $B(\mathrm{IS1})$.

	Expt.	(e, e') [48]	VAP+GCM	
	$B(E\lambda)$ [46]		$B(E\lambda)$	f_{tr}
$E2 : 2_1^+ \to 0_1^+$	7.42 (0.24)	7.79	3.05	1.56
$E2 : 2_1^+ \to 0_2^+$	65 (7)		140	0.68
$E2 : 2_2^+ \to 0_1^+$	0.07 (0.01)	0.05	0.29	0.51
$E2 : 2_2^+ \to 0_2^+$	2.87 (0.72)		0.02	1[a]
$E2 : 2_3^+ \to 0_1^+$	3.59 (1.20)	3.40	2.39	1.23
$E2 : 2_3^+ \to 0_2^+$	7.42 (1.20)		43.7	0.41
$E2 : 4_1^+ \to 2_1^+$	156 (14)			1
$E2 : 4_2^+ \to 2_1^+$	2.39 (0.72)			1
$E2 : 1_1^- \to 3_1^-$	50 (12)		33.7	1.22
$E2 : 1_2^- \to 3_1^-$			1.0	1
$E0 : 0_2^+ \to 0_1^+$	12.6	11.8	12.0	1.03
$E0 : 0_3^+ \to 0_1^+$	16.2	14.2	16.7	0.99
$E0 : 0_4^+ \to 0_1^+$			10.7	1
$E0 : 0_5^+ \to 0_1^+$	10.9		9.0	1.10
$E3 : 3_1^- \to 0_1^+$	205 (11)		207	0.99
$E3 : 3_1^- \to 0_2^+$				1
$E3 : 3_2^- \to 0_1^+$				1
$E3 : 3_2^- \to 0_2^+$				1
$E4 : 4_1^- \to 0_1^+$	378 (133)	420	345	1.10
$E4 : 4_1^- \to 0_2^+$				1
$E4 : 4_2^- \to 0_1^+$		372	71	2.30
$E4 : 4_2^- \to 0_2^+$				1
$\mathrm{IS1}:1_1^- \to 0_1^+$			13.8	1(1.3)[b]
$\mathrm{IS1}:1_1^- \to 0_2^+$			74	1
$\mathrm{IS1}:1_2^- \to 0_1^+$			0.2	1
$\mathrm{IS1}:1_2^- \to 0_2^+$			745	1

[a]The calculated $B(E2 : 2_2^+ \to 0_2^+)$ is too small and therefore is not adjusted to the experimental value but $f_{\mathrm{tr}} = 1$ is used.

[b]For the scaling factor of the $1_1^- \to 0_1^+$ transition, we use $f_{\mathrm{tr}} = 1$ in the default CC calculation and use the modified value $f_{\mathrm{tr}} = 1.3$, which are phenomenologically adjusted so as to reproduce the charge form factors and α-scattering cross sections.

III. α SCATTERING

A. Coupled-channels calculation

Using the matter and transition densities calculated with the VAP + GCM as the input from the structure calculation, we perform the CC calculation of ^{16}O(α, α') with the g-matrix folding model in the same way as in our previous work [16]. The α-^{16}O CC potentials are constructed by folding the
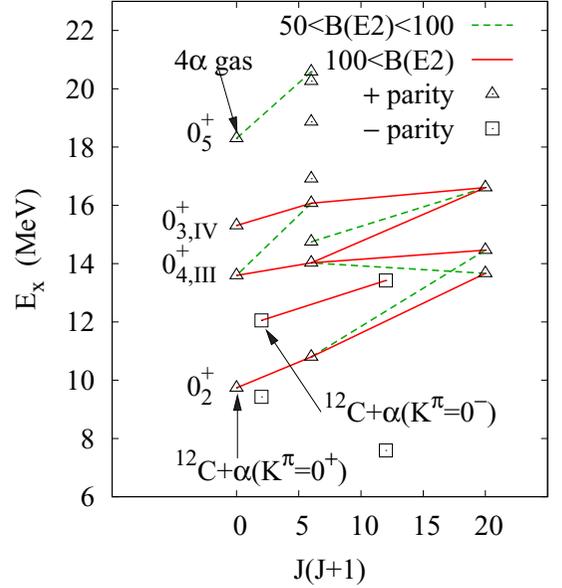
FIG. 2. The energy levels adopted in the CC calculation and the $E2$ transitions. The positive-parity states (0^+, 2^+, and 4^+) are shown by open triangles and the negative-parity states (1^- and 3^-) are shown by open squares. The energy levels are connected by (green) dashed and (red) solid lines in the cases of $50 < B(E2) < 100\ e^2\,\mathrm{fm}^4$ and $B(E2) > 100\ e^2\,\mathrm{fm}^4$, respectively.

Melbourne g-matrix NN interaction [14] with the densities of α and ^{16}O in the approximation of an extended version of the nucleon-nucleus folding model [49]. For the α density, we adopt the one-range Gaussian distribution given in Ref. [50].

In the default CC calculation of the cross sections of the 0^+, 1^-, 2^+, and 3^- states, we adopt the $0_{1,2,3,4,5}^+$, $2_{1,2,3,4}^+$, $1_{1,2}^-$, and $3_{1,2}^-$ states with the $\lambda \leqslant 3$ transitions in the target ^{16}O nucleus. The scaled transition density $f_{\mathrm{tr}}\rho^{(\mathrm{tr})}(r)$ is used. For the excitation energies of ^{16}O, we use the experimental values listed in Table I. In the calculation of the 4^+ cross sections, we adopt $0_{1,2,3,4}^+$, $2_{1,2,3,4,5,6,7,8}^+$, and $4_{1,2,3}^+$ states with the $\lambda = 0, 2, 4$ transitions. For the cross sections to the 0_5^+ state, we also perform the CC calculation using the $0_{1,2,3,4,5}^+$ and $2_{1,2,3,4,5,6,7,8}^+$ states with the $\lambda = 0, 2$ transitions to take into account the strong $E2$ transition between the 0_5^+ and 2_8^+ states and compare the result with the default CC calculation.

B. α-scattering cross sections

The α-scattering cross sections at the incident energies of $E_\alpha = 104$, 130, 146, and 386 MeV are shown in Figs. 5–7, respectively. The cross sections calculated by the Distorted Wave Born Approximation (DWBA) are also shown for comparison.

The elastic cross sections are well reproduced by the present calculation except at large scattering angles for $E_\alpha = 104$–146 MeV. For the $\lambda = 2$ and $\lambda = 3$ transitions to the 2_1^+, 2_3^+, and 3_1^- states, the calculated cross sections are in
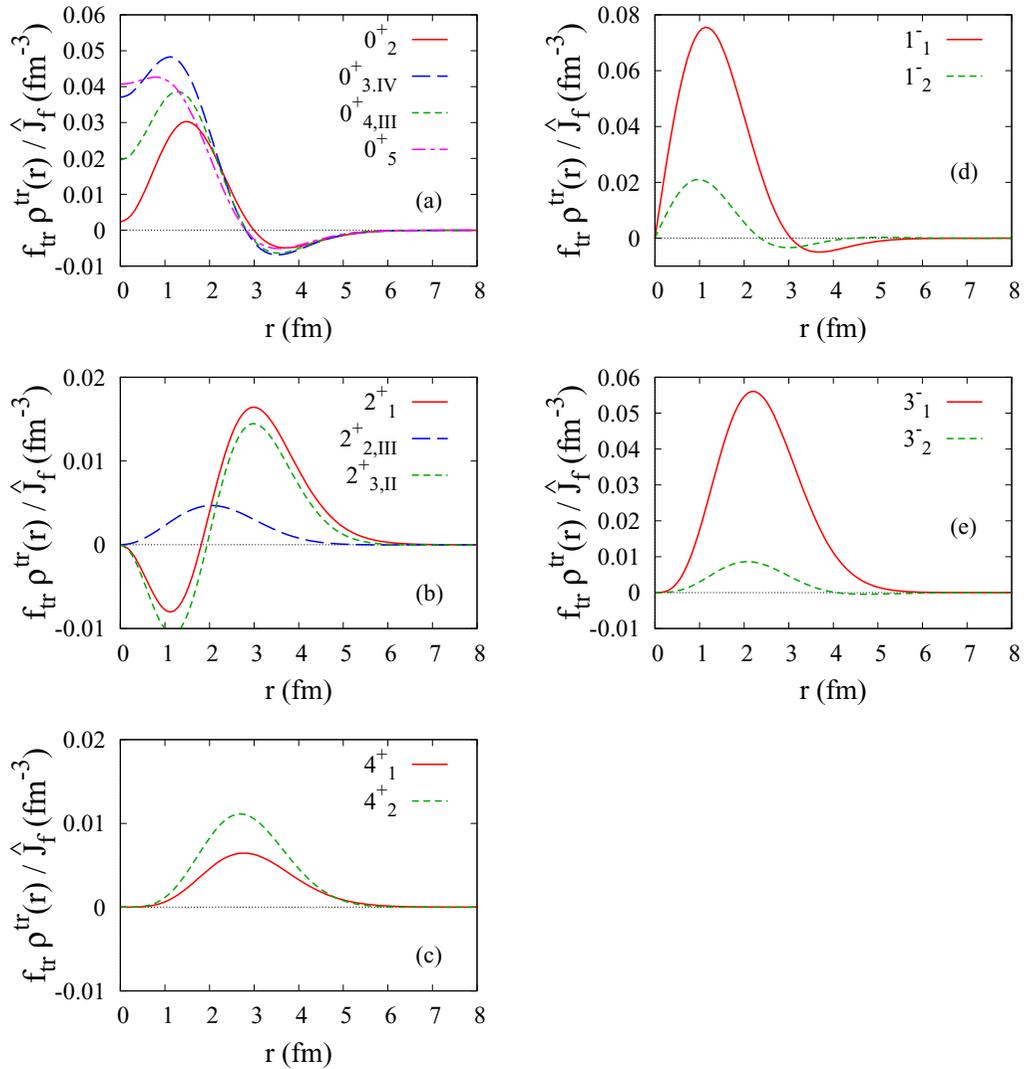
FIG. 3. Transition density for the transitions from the ground state in ^{16}O calculated with the VAP + GCM. The scaled transition density $f_{tr}\rho^{(tr)}(r)$ divided by $\hat{J}_f \equiv \sqrt{2J_f + 1}$ is shown.

good agreement with the experimental data. These states are strongly populated in the direct transitions, and the cross sections are dominantly described by the DWBA calculation. For these states, the CC effect is minor, in particular, at $E_\alpha = 386$ MeV, but not negligible in the cross sections at the relatively low incident energies of $E_\alpha = 104$–146 MeV. For the 2_1^+, the calculation reproduces the absolute amplitude of the cross sections at forward angles but does not satisfactorily describe the diffraction pattern of the observed data. For the 4_1^+ state, the present calculation predicts a very weak population and much underestimates the experimental cross sections.

For the IS dipole excitation to the 1_1^- state, the experimental cross sections are somewhat underestimated by the default CC calculation (solid lines of Fig. 7) with the original $1_1^- \to 0_1^+$ transition density, but successfully reproduced by the calculation with the modified $0_1^+ \to 1_1^-$ transition density scaled by the factor of $f_{tr} = 1.3$, which reproduces the charge form factors of this transition. In comparison with the

DWBA calculation, one can see the significant CC effect in the 1_1^- cross sections. Namely, the absolute amplitude of the cross sections is drastically reduced and the dip positions are slightly shifted to forward angles. This CC effect, which is mainly through the 3_1^- state, is essential to reproduce the first dip position of the experimental cross sections at $E_\alpha = 104$ and 130 MeV.

For the monopole excitations, the calculated 0_3^+ and 0_4^+ cross sections are in good agreement with the observed data. The present CC calculation describes well not only the diffraction pattern but also the absolute amplitude in the wide range of the incident energies of $E_\alpha = 104$–386 MeV, and there is no overshooting problem of the 0^+ cross sections.

In comparison with the DWBA calculation, one can see how the CC effect contributes to the monopole transitions in the α scattering. In the 0_3^+ and 0_4^+ cross sections, the CC effect is not so large but not negligible, in particular, at the low incident energies, $E_\alpha = 104$–146 MeV. By contrast, the
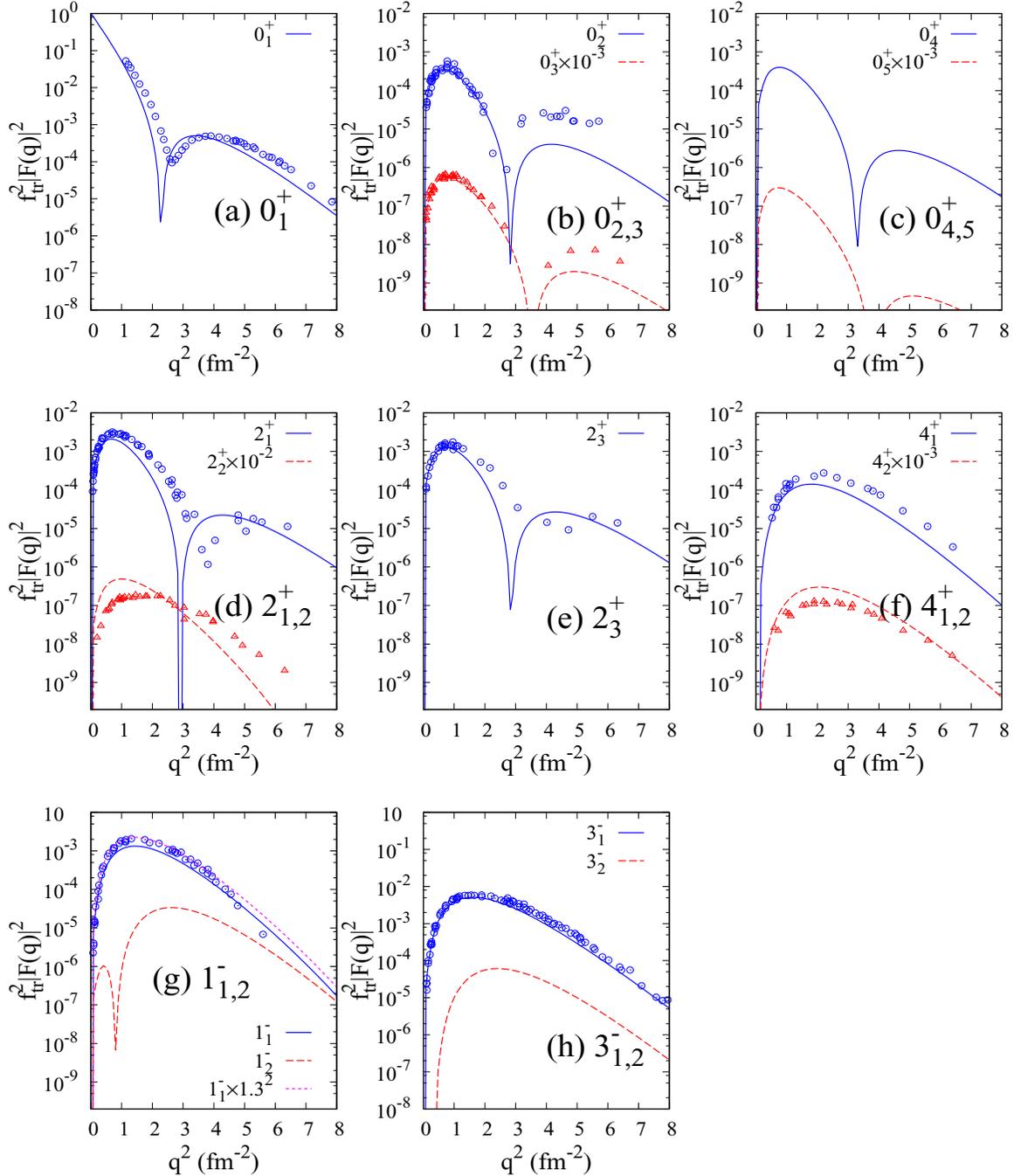
FIG. 4. Squared charge form factors of ^{16}O. The theoretical values obtained with the VAP + GCM are scaled by f_{tr}^2 consistently with the scaled transition density. For the $1_1^- \to 0_1^+$ transition, the squared form factors scaled by the modified value $f_{tr}^2 = 1.3^2$ of the scaling factor are also shown. The experimental data are from Ref. [48].

CC effect gives the drastic change of the 0_2^+ cross sections mainly because of the strong in-band $E2$ transition with the 2_1^- state in the $^{12}C + \alpha$-cluster band built on the 0_2^+ state. At $E_\alpha = 104$–146 MeV, the peak amplitude of the 0_2^+ cross sections is largely reduced by about a factor of three from the result of the DWBA calculation. Even at $E_\alpha = 386$ MeV, the peak amplitude of the CC result is smaller by a factor of two than of DWBA. Also for the 0_5^+ cross sections, the CC effect is found to be of importance, because of the strong $E2$

transitions between the 0_5^+ and 2_8^+ states with the developed cluster structure. Although the CC effect seems to be not so strong in the default CC calculation without the coupling with the higher 2^+ states [the (red) solid lines in Fig. 5], the CC calculation with the $0_{1,2,3,4,5}^+$ and $2_{1,2,\ldots,8}^+$ states shows the drastic CC effect of the significant reduction of the 0_5^+ cross sections at the low incident energies of $E_\alpha = 104$–146 MeV (the (blue) long-dashed lines in Fig. 5). The CC effect in the
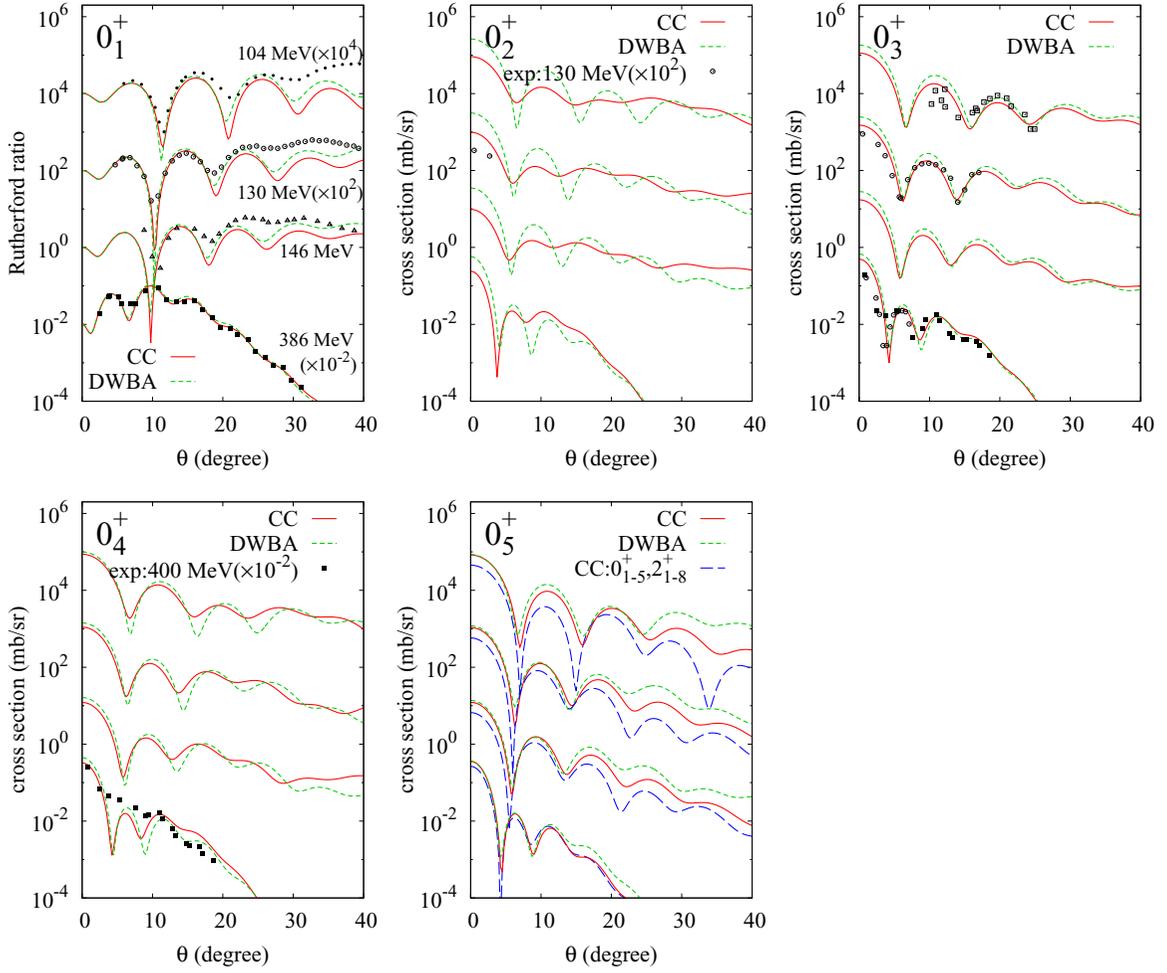
FIG. 5. α-Scattering cross sections on ^{16}O at $E_\alpha = 104$ MeV ($\times 10^4$), 130 MeV ($\times 10^2$), 146 MeV, and 386 MeV ($\times 10^{-2}$). The differential cross sections of the $0^+_{1,2,3,4,5}$ obtained by the CC and DWBA calculations are shown by (red) solid and (green) dashed lines, respectively. For the 0^+_5, the cross sections obtained by the CC calculation using the $0^+_{1,2,3,4,5}$ and $2^+_{1,2,\dots,8}$ states are also shown by (blue) long-dashed lines. The experimental data at $E_\alpha = 104$ MeV [43], 130 MeV [12], 146 MeV [44], and 400 MeV [39] are shown by filled circles, open circles, open triangles, and filled squares, respectively. For the 0^+_3 cross sections, the data at $E_\alpha = 104$ MeV from Ref. [45] and those at $E_\alpha = 386$ MeV from Ref. [12] are also shown by open squares and open circles, respectively.

0^+_5 cross sections becomes weak at the relatively high incident energy of $E_\alpha = 386$ MeV.

In the experimental studies of the monopole transitions, the α-scattering cross sections have been used to deduce the monopole strengths based on the reaction model analysis mainly with the DWBA calculation by naively expecting the scaling law of the α-scattering cross sections and the electric monopole transition strength, $B(E0)$. However, the present analysis of the α scattering indicates that the scaling law is not necessarily valid for the cluster states. First, the amplitude of the 0^+ cross sections can be significantly affected by the CC effect mainly through the strong $\lambda = 2$ transitions between the developed cluster states. Second, the scaling law is not satisfied even in the one-step process of the DWBA cross sections because of the difference in the matter and transition densities between excited 0^+ states. These results indicate that, for study of the monopole transitions by means of the (α, α') reaction, it is necessary to analyze the α-scattering

cross sections with microscopic reaction models considering such the CC effect and density profiles. Nevertheless, we should remark that 0^+ cluster states with significant monopole strengths are strongly populated by the (α, α') reaction, meaning that it is still a good probe for the cluster states and can be useful for qualitative discussion even though the scaling law is not quantitatively valid.

IV. SUMMARY

The α-inelastic-scattering cross sections on ^{16}O was investigated by the folding model with the Melbourne g-matrix NN interaction. This is the first microscopic CC calculation of the ^{16}O(α, α') reaction that is based on the α-nucleus CC potentials microscopically derived with the g-matrix NN interactions and the matter and transition densities of the target ^{16}O nucleus calculated with the microscopic structure model. As for the structure model, we employed the VAP + GCM
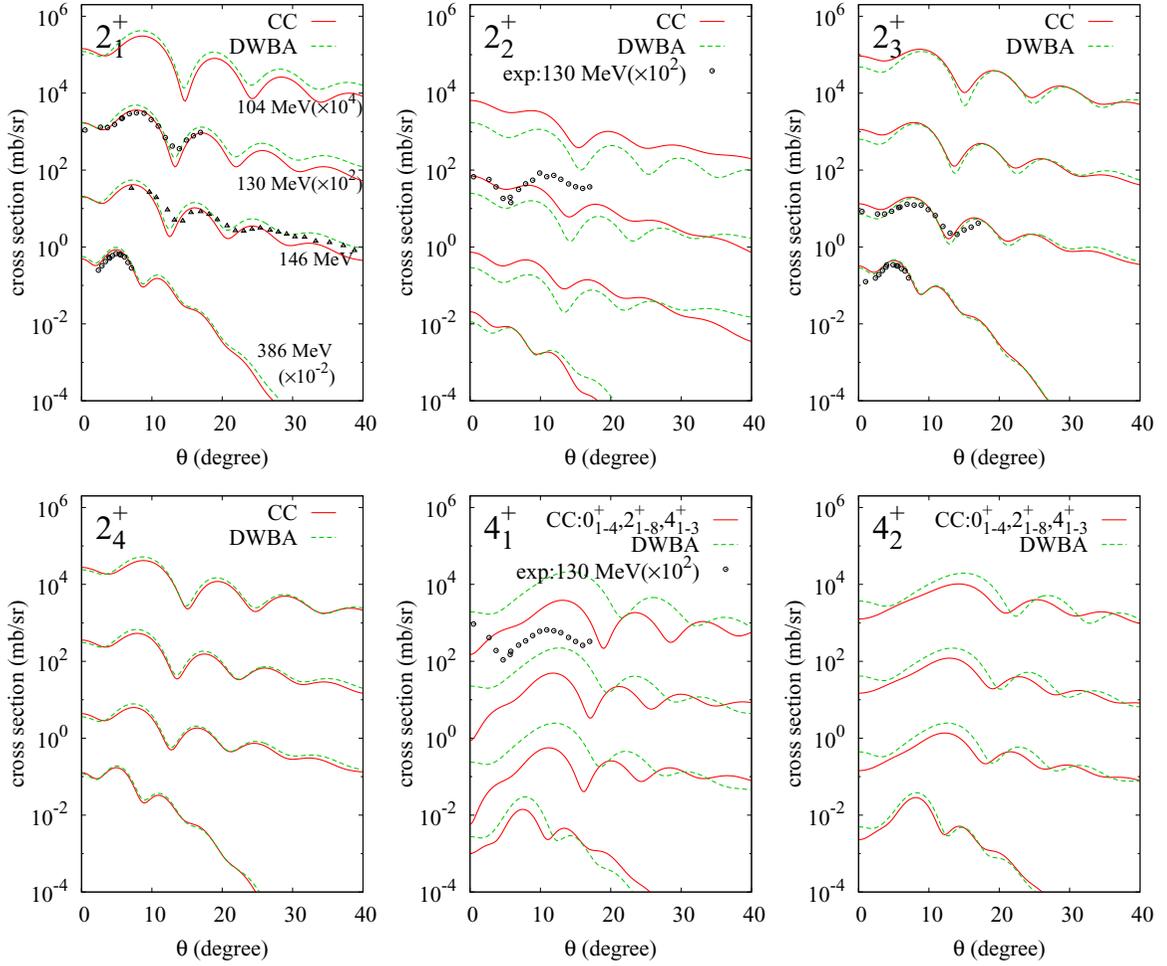
FIG. 6. α-Scattering cross sections on ^{16}O at $E_\alpha = 104$ MeV ($\times 10^4$), 130 MeV ($\times 10^2$), 146 MeV, and 386 MeV ($\times 10^{-2}$). The differential cross sections of the $2^+_{1,2,3,4}$ and $4^+_{1,2}$ obtained by the CC and DWBA calculations are shown by (red) solid and (green) dashed lines. In the CC calculation for the $4^+_{1,2}$ cross sections, the $0^+_{1,2,3,4}$, $2^+_{1,2,...,8}$, and $4^+_{1,2,3}$ states are used. The experimental data at 130 MeV [12], 146 MeV [44], and 386 MeV [12] are shown by open circles, open triangles, and open circles, respectively.

in the framework of the AMD, which is the microscopic approach beyond the cluster models. In the application to the reaction calculation, the calculated transition density is scaled to fit the experimental transition strengths to reduce the ambiguity of the structure model.

The calculation reproduces well the observed cross sections of the $0^+_{2,3,4}$, 2^+_1, 1^-_1, and 3^-_1 states as well as the elastic cross sections at incident energies of $E_\alpha = 104$, 130, 146, and 386 MeV. In the 0^+ cross sections, there is no overshooting problem. In comparison with the DWBA calculation, the significant CC effect was found in the 0^+_2, 0^+_5, and 1^-_1 cross sections because of the strong $\lambda = 2$ coupling between excited states that have developed cluster structures. We clarified that the scaling law of the α-scattering cross sections and $B(E0)$ is not necessarily satisfied for the cluster states because of the significant CC effect through the strong $\lambda = 2$ transitions between the developed cluster states. Nevertheless, it should be remarked that the (α, α') reaction can be used for qualitative discussion on the cluster states because 0^+ cluster states with

significant monopole strengths are strongly populated by the (α, α') reaction.

It is suggested that the microscopic reaction calculation is needed in the quantitative analysis of the α-scattering cross sections. The present g-matrix folding model was proved to be applicable to describe the α-scattering cross sections. This approach is a promising tool to extract information on cluster structures of excited states in other nuclei by the (α, α') reaction.

FIG. 7. α-Scattering cross sections on ^{16}O at $E_\alpha = 104$ MeV ($\times 10^4$), 130 MeV ($\times 10^2$), 146 MeV, and 386 MeV ($\times 10^{-2}$). The differential cross sections of the $3^-_{1,2}$ and $1^-_{1,2}$ obtained by the default CC and DWBA calculations are shown by (red) solid and (green) dashed lines. The experimental data at 104 MeV [45], 130 MeV [12], 146 MeV [44], and 386 MeV [12] are shown by open squares, open circles, open triangles, and open circles, respectively. For the 1^-_1 states, the result calculated with the modified value $f_{\rm tr} = 1.3$ of the scaling factor for the $0^+_1 \to 1^-_1$ transition density are also shown by (magenta) dotted lines.

[1] M. N. Harakeh and A. van der Woude, *Giant Resonances* (Oxford University Press, Oxford, 2001).

[2] T. Kawabata, H. Akimune, H. Fujita, Y. Fujita, M. Fujiwara, K. Hara, K. Hatanaka, M. Itoh *et al.*, Phys. Lett. B **646**, 6 (2007).

[3] T. Yamada, Y. Funaki, T. Myo, H. Horiuchi, K. Ikeda, G. Ropke, P. Schuck, and A. Tohsaki, Phys. Rev. C **85**, 034315 (2012).

[4] Y. Chiba, M. Kimura, and Y. Taniguchi, Phys. Rev. C **93**, 034319 (2016).

[5] B. John, Y. Tokimoto, Y.-W. Lui, H. L. Clark, X. Chen, and D. H. Youngblood, Phys. Rev. C **68**, 014305 (2003).

[6] S. Ohkubo and Y. Hirabayashi, Phys. Rev. C **70**, 041602(R) (2004).

[7] M. Takashina and Y. Sakuragi, Phys. Rev. C **74**, 054606 (2006).

[8] D. T. Khoa and D. C. Cuong, Phys. Lett. B **660**, 331 (2008).

[9] M. Takashina, Phys. Rev. C **78**, 014602 (2008).

[10] M. Itoh *et al.*, Phys. Rev. C **84**, 054308 (2011).

[11] M. Ito, Phys. Rev. C **97**, 044608 (2018).

[12] S. Adachi *et al.*, Phys. Rev. C **97**, 014601 (2018).

[13] K. Minomo and K. Ogata, Phys. Rev. C **93**, 051601(R) (2016).

[14] K. Amos, P. J. Dortmans, H. V. von Geramb, S. Karataglidis, and J. Raynal, Adv. Nucl. Phys. **25**, 275 (2000).

[15] M. Kamimura, Nucl. Phys. A **351**, 456 (1981).

[16] Y. Kanada-En'yo and K. Ogata, Phys. Rev. C **99**, 064601 (2019).

[17] Y. Kanada-En'yo, H. Horiuchi, and A. Ono, Phys. Rev. C **52**, 628 (1995).

[18] Y. Kanada-En'yo and H. Horiuchi, Phys. Rev. C **52**, 647 (1995).

[19] Y. Kanada-En'yo, Phys. Rev. Lett. **81**, 5291 (1998).

[20] Y. Kanada-En'yo and H. Horiuchi, Prog. Theor. Phys. Suppl. **142**, 205 (2001).

[21] Y. Kanada-En'yo, M. Kimura, and A. Ono, PTEP **2012**, 01A202 (2012).

[22] J. A. Wheeler, Phys. Rev. **52**, 1083 (1937); **52**, 1107 (1937).

[23] D. M. Dennison, Phys. Rev. **96**, 378 (1954).

[24] D. M. Brink, H. Friedrich, A. Weiguny, and C. W. Wong, Phys. Lett. B **33**, 143 (1970).

[25] Y. Suzuki, Prog. Theor. Phys. **55**, 1751 (1976).

[26] Y. Suzuki, Prog. Theor. Phys. **56**, 111 (1976).

[27] Y. Fujiwara *et al.*, Prog. Theor. Phys. Suppl. **68**, 29 (1980).

[28] M. Libert-Heinemann, D. Baye, and P.-H. Heenen, Nucl. Phys. A **339**, 429 (1980).

[29] W. Bauhoff, H. Schultheis, and R. Schultheis, Phys. Rev. C **29**, 1046 (1984).

[30] P. Descouvemont, Nucl. Phys. A **470**, 309 (1987).

[31] P. Descouvemont, Phys. Rev. C **44**, 306 (1991).

[32] P. Descouvemont, Phys. Rev. C **47**, 210 (1993).

[33] K. Fukatsu and K. Katō, Prog. Theor. Phys. **87**, 151 (1992).

[34] Y. Funaki, T. Yamada, H. Horiuchi, G. Röpke, P. Schuck, and A. Tohsaki, Phys. Rev. Lett. **101**, 082502 (2008).

[35] Y. Funaki, T. Yamada, A. Tohsaki, H. Horiuchi, G. Röpke, and P. Schuck, Phys. Rev. C **82**, 024312 (2010).

[36] W. Horiuchi and Y. Suzuki, Phys. Rev. C **89**, 011304(R) (2014).

[37] R. Bijker and F. Iachello, Phys. Rev. Lett. **112**, 152501 (2014).

[38] R. Bijker and F. Iachello, Nucl. Phys. A **957**, 154 (2017).

[39] T. Wakasa *et al.*, Phys. Lett. B **653**, 173 (2007).

[40] Y. Kanada-En'yo, Phys. Rev. C **89**, 024302 (2014).

[41] Y. Kanada-En'yo, Phys. Rev. C **96**, 034306 (2017).

[42] Y. Kanada-En'yo and Y. Shikata, arXiv:1903.01075 [nucl-th] [Phys. Rev. C (to be published)].

[43] G. Hauser, R. L'ohken, H. Rebel, G. Schatz, G. W. Schweimer, and J. Specht, Nucl. Phys. A **128**, 81 (1969).

[44] K. T. Knöpfle, G. J. Wagner, H. Breuer, M. Rogge, and C. Mayer-Böricke, Phys. Rev. Lett. **35**, 779 (1975)

[45] M. N. Harakeh, J. R. Comfort, and A. Van der Woude, Phys. Lett. B **62**, 155 (1976).

[46] D. R. Tilley, H. R. Weller, and C. M. Cheves, Nucl. Phys. A **564**, 1 (1993).

[47] I. Angeli and K. P. Marinova, At. Data Nucl. Data Tables **99**, 69 (2013).

[48] T. N. Buti *et al.*, Phys. Rev. C **33**, 755 (1986).

[49] K. Egashira, K. Minomo, M. Toyokawa, T. Matsumoto, and M. Yahiro, Phys. Rev. C **89**, 064611 (2014).

[50] G. R. Satchler and W. G. Love, Phys. Rep. **55**, 183 (1979).